Sensing and Bio-Sensing Research 2 (2014) 49–54

Contents lists available at ScienceDirect

Sensing and Bio-Sensing Research

journal homepage: www.elsevier.com/locate/sbsr

Conformational design optimization of transcription factor beacon DNA biosensors

Stephen R. Schaffner, Kathryn Norquest, Elina Baravik, Jody Stephens, Lisa Fetter, Ryan M. Masterson, Yerelsy Reyna, Andrew J. Bonham *

Department of Chemistry, Metropolitan State University of Denver, Denver, CO 80217, USA

ARTICLE INFO

Keywords:
Transcription factor
Biosensor
Fluorescence

ABSTRACT

Widespread application of promising DNA-based transcription factor protein (TF) biosensors is limited by our ability to control their binding properties. Because the binding properties of this class of biosensors are affected by how well the biosensor switches between binding and non-binding conformations, we investigated the effects of varying conformational stability on the ability of biosensors to detect the oncologically-relevant Myc/Max TF dimer complex. To do this, we employed a custom algorithm that designed and evaluated possible biosensors based on the Myc/Max TF recognition sequence, choosing algorithmic parameters that selected for biosensors with varied conformational stability due to changes in stem length. Biosensors with recognition stem lengths of 8 base pairs (bp), 12 bp, or 21 bp were selected and synthesized. Biosensor binding affinity changes and kinetic association rates were found to be significantly affected by changes in conformational stability (with binding affinity increasing with stem length, from 80 ± 20 nM to 440 ± 80 nM, and kinetic switching rate being tenfold impacted in the longer biosensors). These results show that increased stability can have significant inverse effects on overall biosensor performance, providing important implications for effective biosensor designs. We applied these design insights to generate a biosensor that tested and confirmed a predicted *in vivo* interaction between two TFs (ATF3 and Max), illustrating the potential for rationally-designed, TF-detecting biosensors as a routine analytical tool.

1. Introduction

Improved methods for real-time monitoring of the binding of transcription factor proteins (TFs) to their cognate DNA sites are expected to help elucidate cellular mechanisms [1] and aid in developing novel medical diagnostic tools. To detect interactions between TFs and their cognate DNA sites, DNA-based biosensors have been developed that utilize the ability of DNA to fold in a programmable manner (such as TF beacons [2,3] and DNA microelectrodes [4]). However, adapting these biosensors to different detection ranges or targets remains challenging [5]. As demonstrated by the recent use of DNA aptamer sensors for real-time drug monitoring in living animals [6], such flexibility could open up a new range of point-of-care medical diagnostic possibilities. Recent studies with other DNA-targeting biosensors suggest that improvements in sensitivity and dynamic range can be readily achieved through design optimization [7]. To that end, we investigated here how the conformational stability of TF beacon biosensors affects the DNA-binding affinity and detection range of Myc/Max, a heterodimeric TF complex widely implicated in oncogenesis [8].

Our TF beacon biosensors operate on a population shift mechanism [9] where a single oligonucleotide strand can adopt one of two specific conformations. These conformations affect the biosensor's ability to bind Myc/Max (Fig. 1a). One conformation is a "non-binding" state that occludes the TF recognition site (the consensus "E-box" sequence [10]), inhibiting TF binding. In this conformation, a covalently-bound fluorophore and quencher are in close proximity, allowing for only minimal sample fluorescence. The addition of the target TF can shift the population to a "binding-capable" conformation where the TF recognition site is intact and accessible, allowing TF binding. In this conformation, the fluorophore and quencher are spatially separated, which significantly increases sample fluorescence and results in fluorescent signal that is directly proportional to TF concentration [2].

* Corresponding author. Tel.: +1 303 556 3929.
E-mail addresses: smav26@gmail.com (S.R. Schaffner), k.norquest@gmail.com (K. Norquest), elinabaravik@gmail.com (E. Baravik), jody.stephens@gmail.com (J. Stephens), lisa.fetter18@gmail.com (L. Fetter), ryanmasterson@hotmail.com (R.M. Masterson), yerelsy@gmail.com (Y. Reyna), abonham@msudenver.edu (A.J. Bonham).

http://dx.doi.org/10.1016/j.sbsr.2014.10.007
2214-1804/

The major contributor to stability in the binding-capable state of this class of TF beacon biosensors is likely to stem from an extended, double-stranded DNA (dsDNA) region centered on the recognition site, but it has not been previously investigated how modifying this region affects observed biosensor binding sensitivity. To that end, we designed and created three different TF beacon biosensors directed against the TF complex that vary in the length of dsDNA that flanks the recognition site (Fig. 1b). These designs were determined using a custom scoring computer algorithm that predicts how well a given biosensor will function using UNAFold structure prediction routines [11].

2. Materials and methods

2.1. Reagents and materials

Triton X-100, glycerol, IPTG, AEBSF, Tris base, lysozyme, bovine serum albumin fraction V, HIS-select nickel affinity gel, sodium phosphate, potassium phosphate, sodium chloride, potassium chloride, and magnesium chloride were purchased from Sigma Aldrich (St Louis, MO). DNaseI and BL-21 DE3 competent cells were purchased from New England Biolabs (Ipswich, MA). Biosensors were synthesized by Biosearch Technologies (Novato, CA).

2.2. DNA biosensors

DNA biosensors consist of a single strand of synthetically generated DNA, with 5′ fluorescein amidite (FAM) and an internal blackhole quencher 1 (BHQ1) linked to the C5 position of an internal thymine. Biosensors were synthesized and purified via reverse HPLC. Biosensor sequences for 12 base pair (bp)- and 21 bp-long (“medium” and “long”) recognition stem biosensors were chosen based on a custom algorithmic design process (see Section 2.4. Algorithm development), whereas 8 bp-long (”short”) recognition stem biosensor and ATF3 biosensor were designed manually. The biosensor sequences used in this study are as follows: 8 bp-long biosensor: 5′-FAM-TAA ATT AAC CAC GTG GTT TAT TTT(BHQ1) ATG ATG ACC ACG TGT TCA TCA T-3′; 12 bp-long biosensor: 5′-FAM-CCC GAC CAC GTG GTC GGG T(BHQ1)CC AGA CCA CGT GGT CTG G-3′; 21 bp-long biosensor: 5′-FAM-CCC CCA AGA CCA CGT GGT CTT GGG GGT(BHQ1) CCC CTA GAC CAC GTG GTC TAG GGG-3′; and ATF3 biosensor: 5′-FAM-AGG CGC TGA CGT CAG CGC CT(BHQ1)G AGC TGA CGT CAG CTC AA-3′.

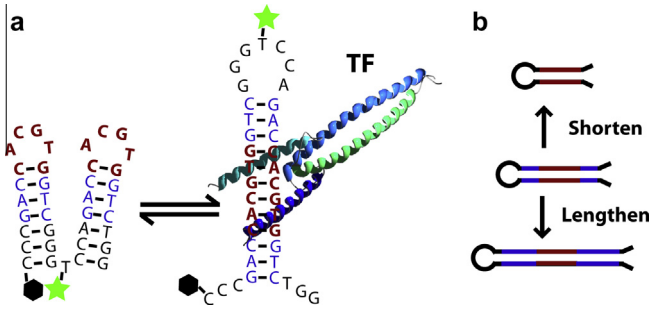

Fig. 1. TF beacon biosensor design and principle of operation. (a) The non-binding, non-fluorescent conformation of the biosensor (left, green fluorophore and black quencher in close proximity) is shifted towards the binding-capable, fluorescent conformation (right, fluorophore and quencher separated) due to binding of the Myc/Max TF complex (blue and green helices) to its DNA recognition site (shown in red). (b) The regions flanking this site (shown in blue) were shortened or lengthened to determine the effects of conformational stability on the binding behavior of the TF complex with the biosensor. (For interpretation of the references to color in this figure legend, the reader is referred to the web version of this article.)

2.3. Protein expression and purification

Recombinant forms of human Myc, Max, ATF3, and TBP were expressed, purified, and characterized as described previously [2,12,13]. Briefly, plasmids were transformed into BL21 strain *Escherichia coli* cells, protein expression was induced via introduction of 0.5 mM IPTG, and cell pellets were collected via centrifugation. Cells were suspended in lysis buffer (50 mM Tris, pH 8.0, 10% glycerol, 0.1% Triton X-100, 100 μg/ml lysozyme, 1 mM AEBSF protease inhibitor, 10 units DNaseI) and ruptured via sonication. Lysate was cleared via filtration through a 0.45 μm filter, and proteins were purified via chromatography with HIS-Select nickel affinity gel. Purity was confirmed via SDS–PAGE and UV–Vis analysis.

2.4. Fluorimetric trials

All fluorescence experiments were conducted at 25 °C in 1× PBS (10 mM sodium phosphate, pH 7.4, 1.8 mM potassium phosphate, 137 mM NaCl, 2.7 mM potassium chloride) with 5 mM $MgCl_2$. Equilibrium and kinetic fluorescence measurements were obtained on a Perkin Elmer LS50B luminescence spectrometer with excitation at 480 (±5) nm and acquisition at 517 (±5) nm unless otherwise specified. Binding curves were obtained using 5 nM biosensor and fit to Langmuir isotherms. Biosensor and buffer were allowed to reach equilibrium in a 16.40F-Q-10 microcuvette from Starna Cells (Atascadero, CA), followed by sequential addition of protein. Solutions were then allowed to reach equilibrium before data was collected. All data was collected in replicate from three to six trials. For kinetics experiments, the same parameters were used but continuous data collection began immediately after addition of protein.

2.5. Algorithm development

We developed a set of Python-based software tools, called Fealden (after the Old English for folding, “fealdan”), that uses an algorithm to search for possible biosensor sequences. The Fealden algorithm uses a depth-first search of a tree of vertexes [14], where each vertex is a candidate biosensor sequence (Fig. 2b). To score each vertex, Fealden takes the candidate sequence and uses UNAFold [11] to perform a theoretical folding calculation. This returns possible conformations of the candidate sequence, including a list of binding pairs and the predicted free energy value for each conformation. Using the binding pair data, Fealden classifies each conformation as either capable of binding the target (i.e., presenting the correct dsDNA region needed for efficient TF binding) or incapable of target binding. Using this classification, along with the predicted free energy values, the algorithm calculates the proportion of each conformation population at equilibrium.

Fealden uses the following properties to classify each conformation’s binding and emission properties (Fig. 2a): a binding-capable conformation must have a single stem, a hairpin loop joining that stem, between 0 and 2 unpaired nucleic acid tails, 100% of the recognition sequence in the dsDNA stem, and a fluorophore and quencher that are at least 4 bases apart; a non-binding conformation must have two stems, hairpin loops joining the ends of each stem, an unpaired bridge joining the two stems, between 0 and 2 tails, less than 50% of the recognition sequence in either stem (to minimize partial binding), and a fluorophore and quencher that are less than 1 nm apart (to maximize quenching of signal). The output from UNAFold does not directly annotate these structural details, so Fealden analyzes this information from the list of binding pairs provided by UNAFold, heuristically “walking” these lists and building them into predicted, two-dimensional folded structures. Using this information, Fealden can classify a given conformation by counting its stems, loops, and tails, using a separate

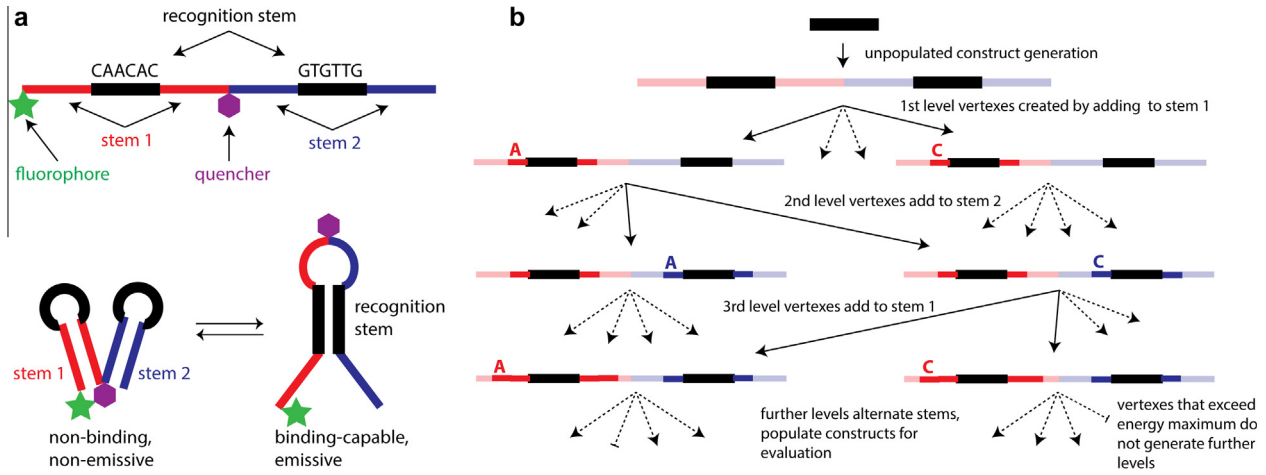

Fig. 2. Fealden search tree structure. (a) The Fealden algorithm uses strong assumptions about TF beacon biosensor conformation, including the formation of a two-hairpin non-binding, non-emissive state (with generated stems 1, red, and 2, blue) and a one-hairpin binding-capable, emissive state (with a stem composed of the recognition element, black). (b) Using this model, our algorithm traverses a tree of candidate biosensor sequences by using the recognition element (black) and then traversing a tree of vertexes with every possible biosensor sequence. To do this, it traverses vertexes, adding bases sequentially and comparing the expected binding energy of the sum of the non-cognate elements (red and blue) to that of the consensus recognition element (black). (Dotted arrows indicate vertexes not shown.) When a vertex whose expected binding free energy in the non-binding, non-emissive conformation exceeds the free energy of the recognition to its complement is found, all descendants of that vertex are not traversed. Candidate sequences identified by this search are then analyzed via UNAFold and characterized further by our algorithm to test for successful biosensor characteristics. (For interpretation of the references to color in this figure legend, the reader is referred to the web version of this article.)

heuristic method to determine rough distances between the fluorophore and quencher, and determining what percentage of recognition sequence is present in each stem.

Since our algorithm relies on strong assumptions about final biosensor structure, we were able to optimize search tree traversal, obtaining multiple order-of-magnitude improvements per total search time. At the root of the search tree is the template for a valid biosensor sequence, which contains three stems: the recognition stem, as well as two additional stems, labeled stem 1 and stem 2 (Fig. 2a). The search tree starts with a cognate recognition element (based on user input or extracted from databases such as JASPAR [15]) and the reverse complement of this element (Fig. 2b, black), which together form the biosensor's recognition stem. When the tree traversal reaches the first level of vertexes, it begins to populate a stem ("stem 1") by randomly placing an A, C, T or G on an end of the recognition element (Fig. 2b). (A reverse complement of this stem is also generated.) Then, on the second level of vertexes, the algorithm generates another new stem ("stem 2") and its complement by adding an A, C, T, or G base to the opposite end of the inherited candidate sequence's recognition element (and reverse complement). As the tree is traversed new bases are added to either stem 1 or stem 2 alternating by level (Fig. 2b). To determine the maximum depth that may still contain effective biosensor sequences, the algorithm calculates the bonding strength of the recognition element to its complement. For our biosensors, optimal performance is obtained when the free energy of the non-binding state (the sum of the free energies of stem 1 and stem 2) have a similar free energy to that of the binding-capable state (which contains a stem composed of the recognition element and its complement) (Fig. 2a) [2]. Our algorithm calculates what the lowest free energy of a given sequence length (e.g., composed of entirely A–T base pairs [bp]) would be that would exceed the recognition sequence's free energy, and then sets that free energy as the maximum search depth (because A–T bp are lower in energy than C–G bp, the longest stem with the lowest energy would be composed entirely of A–T bp). By traversing the tree of vertexes in a depth-first mode but ending a branch when the energy of stem 1 and stem 2 exceeds this threshold, the algorithm has two advantages: it is substantially more likely to generate an effective sequence because it alternates between stem 1 and stem 2, and it dramatically reduces the total search space due to populating new stems and their complements simultaneously.

Fealden traverses vertexes in the search tree until a candidate sequence is scored within a user-specified error range as a functional biosensor. That is, until it finds a sequence satisfying all the requirements for binding-capable and non-binding conformations and free energies of folding. This promising result is then returned to the user, along with useful information, including two-dimensional representations of the highest free energy predicted folds, predicted sensor performance curves, putative equilibrium constant, and the sensor sequence (for example input and output screens, see Supporting information).

3. Results

3.1. Algorithmic sensor design yields functional biosensors

The Fealden algorithm was run on an Ubuntu 12.04 server using the Myc/Max consensus recognition sequence CACGTG [10] with different desired values for overall free energy to optimize towards biosensors with different length stems. Fealden returned the sequences used to generate the biosensors that we refer to as the "medium" (12 bp) and "long" (21 bp) Myc/Max biosensors (the "short" [8 bp] biosensor was a pre-existing construct from prior work [2]) (Fig. 1b). These biosensors were selected from the top sensor results generated by Fealden, without manual curation, and successfully function as TF beacon biosensors comparably to manually designed sensors (Fig. 3a).

3.2. Flanking sequence length affects biosensor affinity

The designed biosensors function robustly when binding to their target, the Myc/Max TF complex. Biosensor apparent affinity was found to vary inversely proportionally to the overall biosensor stability. Specifically, apparent dissociation constants for the TF recognition site were 80 ± 20 nM, 300 ± 70 nM, and 440 ± 80 nM, for the short, medium, and long biosensors, respectively ($n = 5$) (Fig. 3a). These affinities are in line with prior attempts at TF-directed biosensors of this type [2], and reflect the binding-dri-

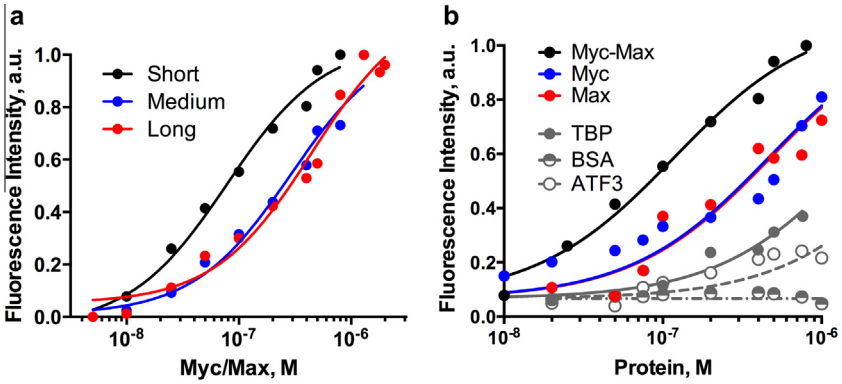

Fig. 3. Myc/Max detection and specificity. (a) Detection sensitivity depends on biosensor stability. Stability of the short (8 bp, black), medium (12 bp, blue), and long (21 bp, red) biosensors increased with length (ΔG of −40.9, −71.2, and −117.7 kJ/mol), while sensitivity decreased with length (80 ± 20 nM, 300 ± 70 nM, and 440 ± 80 nM). (b) Homodimeric and non-specific TF interactions show impacted binding. Myc (blue) or Max (red) in isolation displayed significantly reduced binding across all biosensors (short biosensor response shown in black), consistent with the observed lack of biological activity [16] and poor binding affinities [17] of the homodimeric TFs on the recognition site. The unrelated TF TATA Binding Protein (TBP, gray) and ATF3 (gray circles), as well as bovine serum albumin (BSA, gray half-circles) all displayed negligible binding. (For interpretation of the references to color in this figure legend, the reader is referred to the web version of this article.)

ven population shift between dark and emissive conformations of DNA.

3.3. Biosensors exhibit robust specificity

Our biosensor platform can also analyze relative apparent biosensor binding affinities to different TF complexes, which could be useful for identifying the presence of specific TF combinations. Myc/Max primarily functions as a heterodimer *in vivo*, but studies have suggested that Myc and Max may form homodimers with functional importance in living cells [18]. The affinity of these homodimers for duplex DNA containing their recognition site is not well established, with reported values ranging from negligible [16,17] to greater than the Myc/Max heterodimer [18]. The affinities we observe with our biosensors do not match even these measured affinities to duplex DNA due to the different conformations present in our biosensors, which change the overall energetics of binding. However, we found that when added separately (Fig. 3b), both Myc or Max homodimers exhibit low, but measurable, binding to the biosensors, presumably through homodimer formation [10,18]. This low biosensor binding affinity decreased further with increasing conformational stability. Myc homodimer binding to the short, medium, and long biosensor constructs displayed apparent affinities of 380 ± 120 nM, 440 ± 100 nM, and 1400 ± 300 nM, respectively. Similarly, Max homodimer binding had apparent affinities of 310 ± 80 nM, 380 ± 100 nM, and 540 ± 60 nM for the short, medium, and long biosensors, respectively. As an ideal biosensor should be target-specific and have negligible cross-reactivity with unrelated TFs, we also challenged the biosensors with the nonspecific TFs TATA Binding Protein (TBP) and ATF3, and bovine serum albumin (BSA) (Fig. 3b, gray data). As expected, TBP and ATF3 do not appreciably bind to the biosensor except at concentrations far beyond those relevant for normal detection, and BSA shows no appreciable interaction. These results highlight the specificity of our biosensors for the Myc/Max heterodimer compared to different, but closely related, TF complexes, and suggest that for this, and other systems with varied TF complexes, proper interpretation of signal levels at high protein concentration may be difficult. In future studies, the use of multiple biosensors incorporating unique fluorescent wavelengths tied to differing specificities, recently demonstrated as a means to tune the dynamic range of the sensors [7], could be used as a means of calibration for identifying the signal contribution from multiple, varied TF complexes at high concentrations.

3.4. Biosensor signal kinetics exhibit strong sequence dependence

The dsDNA regions of the binding-capable states that form the short, medium, and long biosensor designs are centered on the recognition site (Fig. 1b). The additional hydrogen bonding in the medium and long biosensors gives greater stability to both the non-binding and binding-capable conformations. The binding-capable states of the short, medium, and long biosensors have predicted ΔG of −40.9 kJ/mol, −71.2 kJ/mol, and −117.7 kJ/mol, respectively. Since the two conformations for each biosensor are iso-energetic ($\Delta\Delta G \approx 0$) and all possess the same recognition sequence, any differences in sensitivity are likely due to kinetic barriers limiting the hydrogen bond breaking involved in one conformation shifting to the other state, where new hydrogen bonds must be made. This kinetic barrier on folding has been studied in other systems, such as simple stem-loop hairpins [19] and larger ribozyme folding patterns [20]. However, kinetic barriers in TF beacon biosensors have not been previously investigated, and this approach differs markedly from studies where only the stability between non-binding versus binding-capable states was analyzed [21].

To investigate the effects of these kinetic barriers, which may limit the efficacy of biosensors, we performed a series of real-time fluorescence experiments (Fig. 4). In these experiments, relatively high concentrations of Myc/Max (either 200 nM or 400 nM) were introduced to 5 nM of either the short or long biosensor and fluorescent signal was continuously measured over time. We found that the kinetic data obtained best fit a sum of two association processes, a protein-dependent rate (constrained to the known value of $2.1 \times 10^5\ M^{-1}$ for Myc/Max association [22]) and a concentration-independent conformational switching rate. Apparent conformational switching rate constants are $170 \pm 10\ s^{-1}$ for the short biosensor and $14 \pm 1\ s^{-1}$ for the long biosensor. These results are limited in that they report only fluorescent gain and do not directly address the separate folding (which includes both hydrogen bond breaking and new hydrogen bond formation) and binding processes present in the biosensors, requiring the use of a previously described association rate as a constraint [22]. However, the differing conformational switching rate constants support our view that the impacted switching kinetics of the longer sensor (relative to the shorter sensor) may reflect a limitation on the ability of the longer sensor to undergo conformational change upon target addition, resulting in a diminished sensor response at a given concentration of target. This suggests that the longer sensor's effective

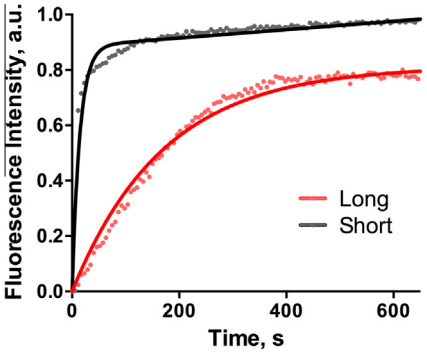

Fig. 4. Short and long sensor designs show significantly impacted kinetics. 200 nM Myc/Max was introduced to either the short (black, 8 bp) or long (red, 21 bp) biosensor, giving a time-dependent increase in fluorescent signal that illustrates the impacted kinetics of the long sensor. Signal was fit to a sum of two association processes, a protein-concentration dependent rate (constrained as $2.1 \times 10^5\ M^{-1}$ from prior measurement [22]) and a concentration-independent conformational switching rate, giving apparent conformational switching rate constants of $170 \pm 10\ s^{-1}$ for the short sensor and $14 \pm 1\ s^{-1}$ for the long sensor. (For interpretation of the references to color in this figure legend, the reader is referred to the web version of this article.)

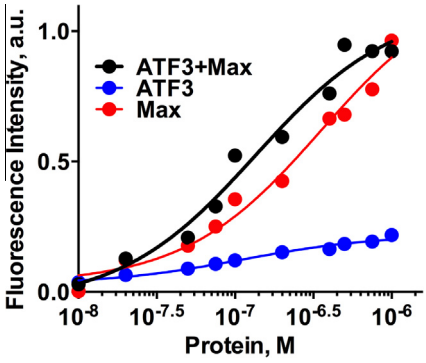

Fig. 5. ATF3 enhances Max binding as predicted. ATF3 in isolation (blue) does not appreciably bind to the biosensor recognition sequence, but enhances the apparent affinity of Max for the short biosensor (black) compared to Max homodimers (red). This supports the existence of previously uncharacterized protein-protein interactions predicted by the ENCODE project [24]. (For interpretation of the references to color in this figure legend, the reader is referred to the web version of this article.)

equilibrium between its conformations has been changed, resulting in the observed different relative apparent affinities for Myc/Max.

These apparent affinities and kinetics data demonstrate that while all biosensors tested responded robustly to Myc/Max, a relatively lower kinetic barrier and higher sensitivity can be achieved using the short biosensor, indicating that shorter flanking sequences are more practical for achieving greater sensitivities. In comparison, the impacted performance of overly stabilized, longer biosensors may be due to interrelated factors including kinetic barriers and differences in the equilibrium across the population of conformations. As part of our design process, all of our biosensors were carefully selected to remove extraneous factors that could interfere with the responses observed. Because the regions flanking the 5′ and 3′ ends of the recognition site can greatly modulate Myc/Max binding affinity, the medium and long biosensors were designed with known high-affinity flanks [10]. Since dehybridization of dsDNA is less favorable with terminal G–C pairs compared to A–T pairs [23], we also designed our biosensors to have invariant G–C rich-regions on the terminal ends of the binding-capable state to minimize differences in apparent affinity. To confirm that the behavior of the sensor alone did not differ substantially from our design, we performed thermal denaturation studies, which strongly suggest that our predicted folding patterns are accurate (see Supporting information). Overall, the significant sequence similarities between the different biosensor designs leave total conformational stability as the primary factor that differs among them. It is worth noting, however, that these factors remain important ones to vary when designing biosensors against other TFs.

3.5. Application of biosensors to confirm predicted binding behavior

Having demonstrated that our biosensors can be designed with robust sensitivity and specificity, we used them to confirm predicted intracellular binding. High-throughput chromatin immune-precipitation (ChIP) studies published as part of the Encyclopedia of DNA Elements (ENCODE) project [24] identified novel protein:protein interaction between Max and ATF3 TFs. To test the validity of this proposed interaction, we tested biosensor binding for Max, Max with added ATF3 protein, and ATF3 (Fig. 5). ATF3 in isolation does not appreciably bind to the biosensors, but improves the binding of Max, with the apparent K_D improving from 310 ± 80 nM to 220 ± 40 nM. This finding validates the ENCODE observation that Max and ATF3 TFs can interact to bind cognate DNA together.

4. Discussion

Changes in the conformational stability of the DNA-based biosensor, based on total dsDNA hydrogen bonding, profoundly affect the sensitivity of the biosensor for its TF target, providing practical size considerations for biosensor designs. This finding presents additional guidance for biosensor optimization and incorporation of biosensors into tools and techniques, such as real-time analyte monitoring in patient blood [6]. Foremost among those observations is that the additional stability offered by longer biosensor designs may in fact significantly limit biosensor performance, favoring smaller biosensor designs. As major challenges remain in the widespread application of biosensors [5], this additional guidance will prove valuable. This study illustrates sensitive affinity measurement of Myc, Max, and the Myc/Max complexes to our biosensors, as well as the validation of a predicted interaction between Max and ATF3 TFs [24], illustrating the diagnostic potential of TF beacon biosensors for conditions such as the upregulation of Myc in a variety of cancers [12]. Finally, given recent advancements using DNA biosensors for *in vivo* monitoring [6], the rational design of TF beacons based on increased understanding of how conformational stability and other key factors influence biosensor performance provides a path forward for successful diagnostic development, such as through future studies establishing the guidelines for the practical limitations on biosensor size due to the observed effects seen with our biosensor designs.

Conflict of interest

The authors declare that there is no conflict of interest.

Acknowledgments

We thank Teisha J. Rowland for helpful discussion and manuscript preparation, and support from the Metropolitan State University of Denver Provost's and Dean's offices.

Appendix A. Supplementary data

Supporting Information available: Fealden web input and output examples and thermal denaturation studies. Supplementary

data associated with this article can be found, in the online version, at http://dx.doi.org/10.1016/j.sbsr.2014.10.007.

References

[1] G.-W. Li, X.S. Xie, Central dogma at the single-molecule level in living cells, Nature 475 (2011) 308–315, http://dx.doi.org/10.1038/nature10315.

[2] A. Vallee-Belisle, A.J. Bonham, N.O. Reich, F. Ricci, K.W. Plaxco, Transcription factor beacons for the quantitative detection of DNA binding activity, J. Am. Chem. Soc. (2011), http://dx.doi.org/10.1021/ja204775k.

[3] A.J. Bonham, K. Hsieh, B.S. Ferguson, A. Valle-Belisle, F. Ricci, H.T. Soh, et al., Quantification of transcription factor binding in cell extracts using an electrochemical, structure-switching biosensor, J. Am. Chem. Soc. 134 (2012) 3346–3348, http://dx.doi.org/10.1021/ja2115663.

[4] A.A. Gorodetsky, A. Ebrahim, J.K. Barton, Electrical detection of TATA binding protein at DNA-modified microelectrodes, J. Am. Chem. Soc. 130 (2008) 2924–2925, http://dx.doi.org/10.1021/ja7106756.

[5] F.S.R.R. Teles, Biosensors and rapid diagnostic tests on the frontier between analytical and clinical chemistry for biomolecular diagnosis of dengue disease: a review, Anal. Chim. Acta 687 (2011) 28–42, http://dx.doi.org/10.1016/j.aca.2010.12.011.

[6] B.S. Ferguson, D.A. Hoggarth, D. Maliniak, K. Ploense, R.J. White, N. Woodward, et al., Real-time, aptamer-based tracking of circulating therapeutic agents in living animals, Sci. Transl. Med. 5 (2013) 213ra165, http://dx.doi.org/10.1126/scitranslmed.3007095.

[7] A. Vallée-Bélisle, F. Ricci, K.W. Plaxco, Engineering biosensors with extended, narrowed, or arbitrarily edited dynamic range, J. Am. Chem. Soc. 134 (2012) 2876–2879, http://dx.doi.org/10.1021/ja209850j.

[8] T. Berg, S.B. Cohen, J. Desharnais, C. Sonderegger, D.J. Maslyar, J. Goldberg, et al., Small-molecule antagonists of Myc/Max dimerization inhibit Myc-induced transformation of chicken embryo fibroblasts, Proc. Natl. Acad. Sci. U.S.A. 99 (2002) 3830–3835, http://dx.doi.org/10.1073/pnas.062036999.

[9] A. Vallee-Belisle, K.W. Plaxco, Structure-switching biosensors: inspired by nature, Curr. Opin. Struct. Biol. (2010) 518–526, http://dx.doi.org/10.1016/j.sbi.2010.05.001.

[10] D.L.C. Solomon, B. Amati, H. Land, Distinct DNA binding preferences for the c-Myc/Max and Max/Max dimers, Nucleic Acids Res. 21 (1993) 5372–5376, http://dx.doi.org/10.1093/nar/21.23.5372.

[11] N.R. Markham, M. Zuker, UNAFold: software for nucleic acid folding and hybridization, Methods Mol. Biol. 453 (2008) 3–31, http://dx.doi.org/10.1007/978-1-60327-429-6_1.

[12] A. Farina, F. Faiola, E. Martinez, Reconstitution of an E box-binding Myc:Max complex with recombinant full-length proteins expressed in *Escherichia coli*, Protein Expr. Purif. 34 (2004) 215–222, http://dx.doi.org/10.1016/j.pep.2003.11.021.

[13] B.P. Chen, C.D. Wolfgang, T. Hai, Analysis of ATF3, a transcription factor induced by physiological stresses and modulated by gadd153/Chop10, Mol. Cell. Biol. 16 (1996) 1157–1168.

[14] R. Tarjan, Depth-first search and linear graph algorithms, SIAM J. Comput. 1 (1972) 146–160, http://dx.doi.org/10.1137/0201010.

[15] J.C. Bryne, E. Valen, M.H.E. Tang, T. Marstrand, O. Winther, I. da Piedade, et al., JASPAR, the open access database of transcription factor-binding profiles: new content and tools in the 2008 update, Nucleic Acids Res. 36 (2008) D102–D106, http://dx.doi.org/10.1093/nar/gkm955.

[16] C.V. Dang, J. Barrett, M. Villa-Garcia, L.M. Resar, G.J. Kato, E.R. Fearon, Intracellular leucine zipper interactions suggest c-Myc hetero-oligomerization, Mol. Cell. Biol. 11 (1991) 954–962, http://dx.doi.org/10.1128/MCB.11.2.954.

[17] A.J. Bonham, N. Wenta, L.M. Osslund, A.J. Prussin II, U. Vinkemeier, N.O. Reich, STAT1 DNA-sequence dependent binding modulation by phosphorylation, protein:protein interactions, and small molecule Inhibition, Nucleic Acids Res. 41 (2012) 754–763, http://dx.doi.org/10.1093/nar/gks1085.

[18] K.C. Jung, H.S. Rhee, C.H. Park, C.H. Yang, Determination of the dissociation constants for recombinant c-Myc, Max, and DNA complexes: the inhibitory effect of linoleic acid on the DNA-binding step, Biochem. Commun. 334 (2005) 269–275, http://dx.doi.org/10.1016/j.bbrc.2005.06.088.

[19] W. Zhang, S.-J. Chen, RNA hairpin-folding kinetics, Proc. Natl. Acad. Sci. U.S.A. 99 (2002) 1931–1936, http://dx.doi.org/10.1073/pnas.032443099.

[20] D.K. Treiber, M.S. Rook, P.P. Zarrinkar, J.R. Williamson, Kinetic intermediates trapped by native interactions in RNA folding, Science 279 (1998) 1943–1946, http://dx.doi.org/10.1126/science.279.5358.1943.

[21] A. Vallée-Bélisle, F. Ricci, K.W. Plaxco, Thermodynamic basis for the optimization of binding-induced biomolecular switches and structure-switching biosensors, Proc. Natl. Acad. Sci. U.S.A. 106 (2009) 13802–13807, http://dx.doi.org/10.1073/pnas.0904005106.

[22] S. Park, S. Chung, K.-M. Kim, K.-C. Jung, C. Park, E.-R. Hahm, et al., Determination of binding constant of transcription factor myc-max/max-max and E-box DNA: the effect of inhibitors on the binding, Biochim. Biophys. Acta 1670 (2004) 217–228, http://dx.doi.org/10.1016/j.bbagen.2003.12.007.

[23] Y. Yin, X.S. Zhao, Kinetics and dynamics of DNA hybridization, Acc. Chem. Res. 44 (2011) 1172–1181, http://dx.doi.org/10.1021/ar200068j.

[24] S. Neph, J. Vierstra, A.B. Stergachis, A.P. Reynolds, E. Haugen, B. Vernot, et al., An expansive human regulatory lexicon encoded in transcription factor footprints, Nature 489 (2012) 83–90, http://dx.doi.org/10.1038/nature11212.